

Journal of Materials Chemistry A

Accepted Manuscript



This is an *Accepted Manuscript*, which has been through the Royal Society of Chemistry peer review process and has been accepted for publication.

Accepted Manuscripts are published online shortly after acceptance, before technical editing, formatting and proof reading. Using this free service, authors can make their results available to the community, in citable form, before we publish the edited article. We will replace this *Accepted Manuscript* with the edited and formatted *Advance Article* as soon as it is available.

You can find more information about *Accepted Manuscripts* in the [Information for Authors](#).

Please note that technical editing may introduce minor changes to the text and/or graphics, which may alter content. The journal's standard [Terms & Conditions](#) and the [Ethical guidelines](#) still apply. In no event shall the Royal Society of Chemistry be held responsible for any errors or omissions in this *Accepted Manuscript* or any consequences arising from the use of any information it contains.



Journal Name

ARTICLE

Quantitative relation between photocatalytic activity and degree of <001> orientation for anatase TiO₂ thin films

Received 00th January 20xx,
Accepted 00th January 20xx

DOI: 10.1039/x0xx00000x

www.rsc.org/

Bozhidar I. Stefanov, Gunnar A. Niklasson, Claes G. Granqvist and Lars Österlund*

We demonstrate a quantitative relation between exposed crystal surfaces and photocatalytic activity of nanocrystalline anatase TiO₂. Thin films with controlled amount of <001> preferential orientation were prepared by reactive DC magnetron sputtering in Ar/O₂ atmosphere with the partial O₂ pressure as control parameter. The samples were characterized with X-ray diffraction, transmission electron microscopy and atomic force microscopy, from which the degree of preferential <001> orientation and exposed facets were determined by an extension of the March-Dollase model. Photocatalytic degradation of methylene blue dye shows that the photocatalytic reaction rate increases approximately with the square of the fraction of <001> oriented surfaces, with about eight times higher rate on the {001} surfaces, than on {101}, thus quantifying the effect of crystal facet abundance on the photocatalytic activity of anatase TiO₂.

Introduction

The chemical reactivity of TiO₂ is known to depend strongly on its surface structure and morphology.¹⁻³ In particular, the {001} surfaces of anatase TiO₂ have been shown to be associated with high reactivity.⁴⁻⁵ Accordingly, a number of methods have been proposed to prepare chemically reactive TiO₂ materials, including e.g. laser ablation,⁶ modification of surface acidity,³ and hydrophilicity through chemical and mechano-chemical methods.⁷ Recently, preparation of TiO₂ with controlled crystallographic properties, such as facet distribution and preferential orientation, has attracted considerable attention.⁸⁻¹¹ In particular, the study by Yang et al. of F⁻ ion assisted shape-controlled synthesis of {001} exposed TiO₂ particles has spurred interest in this field.¹²

Normally anatase nanoparticles are dominated by low-energy {101} surface planes with only a fraction of {001} facets, typically about 10% of the total surface area.¹³ It has been predicted that the {001} facets are much more reactive than the {101} facets due to their higher surface energy (0.9 J m⁻² versus 0.44 J m⁻² for {101}).¹⁴ Theoretical work has shown that water and other small molecules, such as methanol and formic acid, adsorb molecularly on {101} surfaces while dissociation is favoured on {001} surfaces.^{4,5,15} Furthermore it was observed that the {001} and {101} surfaces exhibit selectivity towards oxidation and reduction reactions, respectively.^{16,17} These

observations suggest that it is possible to purposefully tailor-make TiO₂ materials with improved reactivity. It is, however, challenging to experimentally prepare nanostructured TiO₂ with different facet distributions and quantify the facet-controlled reactivity. Several studies have shown that reactive DC magnetron sputtering yields anatase TiO₂ films with preferential orientation along the <001> crystallographic direction.¹⁶⁻¹⁹ Depending on the preparation conditions, this orientation might be altered. For example if the films are deposited at high temperature, leading to direct formation of anatase, substrate bias can be used to change the crystallographic orientation.¹⁹ In the case of room temperature deposition, yielding initially amorphous films with varying stoichiometry, growth in the <001> direction can be induced by post-deposition heat treatment.^{17,19} This textured growth is an intrinsic property of the films and is unaffected by the type of substrate that is used.¹⁷ We have previously demonstrated that the preferential <001> orientation of the crystal grains in nanostructured films can be controlled by altering the partial oxygen pressure in the deposition chamber during thin-film preparation.²¹⁻²²

In this work we systematically vary the fraction of {001} planes in anatase TiO₂ films and show that their photo-reactivity follows a quadratic functional dependence as a function of exposed {001} surface area. Apart from providing experimental quantification of facet reactivity, our results can be used to predict photocatalytic reaction rates from structural properties of nanostructured TiO₂ materials.

Experimental part and methods

Eight sets of samples with increasing <001> preferential orientation were deposited by reactive DC magnetron

^a Address here.

^b Address here.

^c Address here.

† Footnotes relating to the title and/or authors should appear here.

Electronic Supplementary Information (ESI) available: [details of any supplementary information available should be included here]. See

DOI: 10.1039/x0xx00000x

sputtering, in a system based on a Balzers UTT 400 unit, as described in detail elsewhere (Figure 1a).²³ The substrates (standard microscopy slide glass substrates, Thermo Fischer Scientific, USA) were rotated during deposition in order to assure thickness uniformity. Depositions were done on unheated substrates in 20 mTorr Ar/O₂ atmosphere using two 5-cm-diameter Ti targets (99.995% Ti, Plasmaterials, CA, USA) at fixed current of 0.75 A. The size of the coated area was approx. 50 × 25 mm. The partial O₂ pressure (0.55 < P_{O₂} < 1.55 mTorr) during deposition was used as control parameter to purposefully adjust the preferential crystal orientation of the post-annealed films. The sputtering time was held fixed, and a slight increase of the sputtering rate (from 16 to 19 nm min⁻¹) proportional to P_{O₂} was observed. After deposition the films were post-annealed for 1h at 500°C in air (Figure 1b).²¹

To exclude the possibility of any influence of target history on ensuing film properties, two different sets of Ti targets were employed: one set of two new targets and another set which had been extensively used and hence exhibited clear “race-track” features.²⁴

Film thicknesses were between 573 and 696 nm, as determined by surface profilometry (Dektak XT Advance, Bruker).

Surface morphology was observed by atomic force microscopy (AFM) employing a PSIA XE150 SPM/AFM instrument (Park Systems, Suwon, Korea), operating in non-contact mode. Silicon cantilevers (ACTA, AppNano) with tip radius in the range 6 – 10 nm were used. Morphological data was determined based on six images, captured at random points on the film.

Transmission electron microscopy (TEM) images were obtained using a JEOL 2000 FX II STEM operating at 200 kV in TEM mode. Samples were prepared by scraping the film off the substrate and dispersing in chloroform (puriss. >99%, Sigma Aldrich, MO, USA). A holey carbon grid was then dipped into the suspension. Due to the columnar growth of the film, it would easily break in the growth direction so that pieces exhibiting cross-section view are visible on the grid.

The crystal structure and preferential orientation of the grains in the films were determined by Grazing Incidence X-Ray Diffraction (GIXRD; Siemens D5000 diffractometer employing CuK_{α1} radiation at 0.5° incidence angle). The amount of <001> orientation was quantified via Rietveld refinement of XRD data using the PowderCell package,²⁵ and the March-Dollase (MD) model was used for quantification of the texturing.²⁶ The MD function, W(α), is used for adjusting the intensity ratio of peaks in the fitted XRD pattern until it describes the experimental one. The MD weight-function is defined as:

$$W(\alpha) = (MD_{\langle hkl \rangle}^2 \cos^2 \alpha + \frac{1}{MD_{\langle hkl \rangle}} \sin^2 \alpha)^{-3/2}, \quad (1)$$

where MD_{<hkl>} is the March-Dollase parameter for the <hkl> direction, and α is the angle, in radians, between the preferential orientation vector and the surface plane of the film. The MD parameter is 1 for randomly oriented films and decreases proportionally to the amount of preferential

orientation. As shown in Figure 2, a decreasing MD_{<hkl>} leads to an increased probability of finding crystallites with the <001> direction perpendicular to the surface.

The MD parameter can be converted into a degree of preferred orientation, η_{<hkl>}, by means of Zolotoyabko's equation.²⁷ Here η_{<hkl>} is defined as the percentage of excess of crystallites with preferential orientation, compared to the situation in a film with randomly oriented crystallites. The amount of crystallites is estimated by normalizing the integral of W(α) over a given range of angles. In Zolotoyabko's model this range is -π/6 < α < π/6 (±30°). The excess orientation, compared to random orientation, is then defined as:

$$\eta_{\langle hkl \rangle} = \frac{\int_{-\pi/6}^{\pi/6} (W(\alpha) - 1) d\alpha}{\int_{-\pi/2}^{\pi/2} W(\alpha) d\alpha} \times 100\%, \quad (2)$$

Note that in eq. 2 only the excess of oriented particles is integrated; the value of W(α) for a random film (W(α) = 1) is subtracted in the numerator. The integral can be solved analytically and the result is:

$$\eta_{\langle hkl \rangle} = \sqrt{\frac{(1 - MD_{\langle hkl \rangle})^3}{(1 - MD_{\langle hkl \rangle}^{-3})}} \times 100\%, \quad (3)$$

where MD_{<hkl>} is obtained from the Rietveld refinement procedure.

Spectrophotometry was performed with a Perkin-Elmer Lambda 900 spectrophotometer equipped with a 150 mm BaSO₄ coated integrating sphere. Transmission spectra were recorded in the 300 < λ < 800 nm wavelength region.

The photocatalytic activity of the films was measured by photocatalytic oxidation of methylene blue (MB) dye (biological grade, Sigma Aldrich, USA), 1 ppm in water. The measurements were carried out in a custom-built reactor wherein the concentration of the dye in the solution is measured *in situ* by laser colorimetry at λ = 670 nm.²⁸ Each experiment comprised an initial 40 minutes of adsorption, which was needed to reach adsorption-desorption equilibrium. Subsequently a black-light UV tube was used to illuminate the films (2.44 mW cm⁻² at the film surface), and the dye concentration was measured *in situ* every 10 min for 80 min.

Results

Figure 3 shows photographs of as-deposited films. The films were transparent at high values of P_{O₂}, but an increasing blue tint, which signals sub-stoichiometry, was observed at low P_{O₂} in the sputtering process. The tint disappeared during the heat-treatment, as the films were oxidized. The stoichiometry of the films, deposited at low, medium and high P_{O₂} was compared by EDX in a previous study and the Ti:O ratio was, as expected, found to be 1:2, and consistent for all samples.²¹

A correlation was found between the stoichiometry of the as-deposited films and the orientation of the crystalline grains after heat treatment. This correlation is attributed to variations of nucleation sites for crystal growth whereby sputtering at low P_{O₂} introduces oxygen-poor regions which

promote nucleation in random directions, thus effectively lowering η_{001} . This correlation was observed both for the new and used targets. Albeit the sputtering pressure regimes were slightly different due to the different active target areas, the same control of η_{001} was achieved, and η_{001} was in both cases found to be linearly proportional to P_{O_2} (Figure 4).

Analysis of AFM images showed no morphological changes in films prepared with different P_{O_2} (Figure 5). The values for the average rms roughness (r_{rms}) obtained by AFM are listed in Table 1 and are not strongly affected by P_{O_2} .

The XRD diffractograms in Figure 6 show that as-deposited films are amorphous. Upon heating, these films were converted into polycrystalline TiO_2 consisting of pure anatase phase, as apparent from its characteristic reflections.²⁹ With increasing P_{O_2} , the relative intensity of the peaks in the XRD pattern, associated with $\langle 001 \rangle$ orientation, is observed to increase. Mean crystallite size was also obtained from the XRD data and showed a slight decrease of the crystal size as a function of P_{O_2} , from 24 to 18 nm diameter (Table 1).

Measuring the optical properties of TiO_2 films, especially the refractive index, provide means to estimate the film porosity. Refractive indices of the films were determined from optical transmission spectra shown in Figure 7, using the envelope method suggested by Swanepoel.³⁰ The maxima and minima of the interference fringes of the transmittance spectrum were fitted with a set of spline functions, enveloping the spectrum, as depicted in Figure 7. The refractive index was then calculated from

$$n = [N + (N^2 - s^2)^{1/2}]^{1/2}, \quad (4)$$

where s is the refractive index of the substrate and N is defined as

$$N = 2s \frac{T_{max} - T_{min}}{T_{max} + T_{min}} + \frac{s^2 + 1}{2}. \quad (5)$$

Here T_{max} and T_{min} are the values of the maximum and minimum envelope functions of the transmittance at a given wavelength. The refractive index of the substrate was calculated using

$$s = \frac{1}{T} + \left(\frac{1}{T^2} - 1 \right)^{1/2}, \quad (6)$$

where T is the transmittance of an uncoated substrate at a given wavelength. Our glass substrates were characterized by $s = 1.53$ (averaged over the $500 < \lambda < 700$ nm range). The refractive indices of the TiO_2 films were determined from the averaged refractive index over all visible maxima and minima, except the ones near the band gap where the decrease in transmittance affects the interference fringes. Values of n were obtained as an average over the wavelengths indicated in Figure 7, and are given in Table 1.

The packing densities, ρ , of the two samples were then estimated using the Pulker equation,³¹

$$\rho = \frac{\rho_f}{\rho_b} = \frac{n_f^2 - 1}{n_f^2 + 2} \cdot \frac{n_b^2 + 2}{n_b^2 - 1}, \quad (7)$$

where ρ_f and ρ_b are the film and the bulk density of the material, and n_f and n_b are the film and bulk refractive index, respectively ($n_b = 2.56$ was used for the refractive index of anatase)³². Packing densities are also given in Table 1.

Figure 8 shows the MB concentration in the solution as a function of time, where UV illumination is started after 40 min, for a TiO_2 film prepared at $P_{O_2} = 1.53$ mTorr corresponding to $\eta_{001} = 38\%$. Two parameters were determined from the photocatalytic measurements: (i) the saturation coverage of MB adsorbed without illumination (C_{sat}^{MB}) (40 min period prior to illumination) and (ii) the MB oxidation rate (k_{MB}).

The saturation coverage C_{sat}^{MB} was extracted from the adsorption isotherm

$$C_{MB} = C_{sat}^{MB} (1 - e^{-k_{ad}t}), \quad (8)$$

and used as a figure-of-merit of the number of adsorption sites for the films, or their effective surface areas. Here C_{MB} is the amount of dye, adsorbed on the surface, at time t . It is obtained from the decrease of MB in the solution ($1 - C/C_0$) during the adsorption in dark, where C and C_0 are the concentrations of MB in the liquid phase at time t and the initial concentration (1 ppm), respectively (both proportional to the optical absorbance of the dye). C_{sat}^{MB} is the calculated saturation coverage, and k_{ad} is the adsorption rate.

The photocatalytic MB degradation rate, k_{MB} , was calculated from the decreasing absorbance at $\lambda = 670$ nm, assuming that the reaction obeyed pseudo-first order kinetics, viz.

$$-\log(C/C_0^{UV}) = k_{MB}t, \quad (9)$$

where C_0^{UV} is the MB concentration at the time at which the UV lamp was turned on. Figure 9 shows examples of three such kinetic plots for films with increasing η_{001} . Clearly the rate increases with increasing η_{001} .

To further quantify the effect of the $\langle 001 \rangle$ orientation on the photocatalytic rate, measurements were performed on eight sets of films with increasing degree of orientation. Each set consisted of four samples, deposited in two batches. Kinetic rate constants (Table 1) were averaged over the four measurements, and clearly show large dependence on the degree of preferential $\langle 001 \rangle$ orientation.

Discussion

The dependence of k_{MB} on preferential orientation was modelled assuming that the rate of MB photo-degradation can be described by contributions from two sites – either $\{101\}$ sites or $\{001\}$ sites – whose sum accounts for the total number of active sites on the photocatalyst.

While it is viable to use η_{001} for quantification of the preferential orientation, it is not appropriate to relate it to facet-specific photocatalytic activity, since η_{001} is defined as

an excess of oriented particles, not the absolute fraction of {001} facets.

Hence we introduced another parameter, denoted A_{001} , which is obtained by integrating $W(\alpha)$ within a defined region around the <001> direction where other low-index planes do not contribute. Noting that the <101> direction is 45° from the <001> direction, we apply a narrower integration range, between $-\pi/18 < \alpha < \pi/18$ ($\pm 10^\circ$) than that used in Zolotoyabko's approach, to avoid contributions from {101} reflections. Thus we obtain

$$A_{001} = \frac{\int_{-\pi/18}^{\pi/18} W(\alpha) d\alpha}{\int_{-\pi/2}^{\pi/2} W(\alpha) d\alpha} \cdot 100\%, \quad (10)$$

where the normalization yields the relative area of exposed {001} surfaces. This procedure is based on the assumption that particles, oriented within the range $\pm\pi/18$ ($\pm 10^\circ$) of the <001> direction, yield {001} surfaces and all the rest - {101} facets. From eq. 10 it follows that random orientation corresponds to $A_{001} = 11\%$, which is in agreement with previous reports.¹³

Figure 10 shows data on k_{MB} as a function of A_{001} for the complete set of films. k_{MB} increases non-linearly as a function of the amount of <001> orientation, which suggests that the fraction of exposed {001} to {101} surfaces is the governing parameter for film reactivity. Using a two-surface-facet model with separate reaction rates associated with each facet, the reaction rate can thus be described by

$$k_{MB} = k_{101}(1 - A_{001})^x + k_{001}(f_{001}A_{001})^x \quad (11),$$

where k_{101} and k_{001} are the reaction rates on the {101} and {001} facets, respectively. Here we assume that increasing A_{001} leads to proportionally more exposed {001} facets, and conversely to a corresponding decrease of exposed {101} surfaces. Furthermore x is the reaction order and f_{001} is a factor to compensate for the higher density of active sites on the {001} surface. The Ti atom surface density on the {101} and {001} surfaces are 5.17×10^{14} and $6.99 \times 10^{14} \text{ cm}^{-2}$, respectively, yielding $f_{001} = 1.35$. The dashed curve in Figure 10 shows a least-square fit to the experimental data, which yields $k_{101} = 0.99$, $k_{001} = 7.56$ and $x = 2.05$. Thus the apparent MB photo-degradation rate is approximately 8 times larger on {001} surfaces than on {101} surfaces. Furthermore, the photocatalytic rate increases approximately with the square of the amount of preferential <001> orientation. The quadratic increase of reaction rate can be attributed to the increasing fraction of {001} surfaces.

To explore other possible contributions to the non-linear increase of k_{MB} as a function of A_{001} , we scrutinized the influence of microstructural changes of the films which may result in increased porosity at higher P_{O_2} thereby yielding a larger number of active surface sites. As is evident from Table 1, ρ is large for all films and this shows that the films are rather dense. The packing density is, however, decreased from 92% to 81% with increasing P_{O_2} as n drops from 2.34 to 2.09, i.e. a larger porosity is obtained for increasing P_{O_2} . The total change in porosity of about 11% is, however, much too small to

account for the non-linear increase of the reaction rate in Figure 10. Moreover, the differences in porosity are not observed in the AFM images (Figure 5). The surface roughness is of the order of $1.3 \pm 0.1 \text{ nm}$, and no correlation with P_{O_2} was observed. The films exhibit surface morphology typical for sputter deposited samples and manifested in structure zone diagrams.³³ The films surfaces are seen to consist of densely packed spherical protrusions with in-plane dimensions of about 100 nm and heights of a few nanometers. The morphology seen in AFM is in line with cross-section TEM data (Figure 1c), which show dense films exhibiting columnar growth. Furthermore, the measured saturation coverage for each film is not dependent on P_{O_2} . We conclude that the variations in ρ deduced from the changes in refractive index mainly are associated with enclosed pores within the films, which are not accessible to MB adsorption. Further evidence that the increased porosity does not contribute significantly to the photocatalytic activity can be found in Table 1 for films prepared by differently aged sputter targets. The aged targets yielded lower sputtering yields, and since the sputtering time was kept fixed this yields thinner films (marked with asterisks in Table 1). The observed reactivity is seen to fit the functional dependence of the preferred orientation in Figure 10. Hence we can conclude that we are in a region where the thickness does not contribute to the photocatalytic activity and that any pores enclosed in the volume are not accessible to the MB dye.

Hence the main contribution to the non-linear increase of the reactivity of the films is an increasing fraction of exposed {001} surfaces. Other contributions, such as increased porosity and decreasing crystallite sizes in films with increasing P_{O_2} , are not expected to contribute significantly.

Conclusions

In summary, we have demonstrated that the photocatalytic activity of TiO_2 is strongly dependent on the nature and reactivity of the exposed surface facets. Increasing the amount of preferential <001> orientation enhances the photocatalytic oxidation rate of MB dye approximately quadratically, and the newly exposed {001} facets exhibit about 8 times higher reactivity per active surface site in this reaction. To our knowledge this is the first quantification of the effect of varying crystal facets of TiO_2 nanocrystals. Furthermore, we have demonstrated the possibility to use reactive DC magnetron sputtering in order to prepare polycrystalline anatase TiO_2 films with precise control of the crystallographic orientation. This technique can be used in other similar studies to elucidate the reactive nature of crystallographic planes in TiO_2 as well as in technical applications embracing the industrial upscaling viability of the sputtering technology.

Acknowledgements

This work was funded by the European Research Council under the European Community's Seventh Framework Program

(FP7/2007-2013)/ERC Grant Agreement No. 267234 ("GRINDOOR").

Notes and references

- P. A. M. Hotsenpiller, J. D. Bolt, W. E. Farneth, J. B. Lowekamp and G. S. Rohrer, *J. Phys. Chem. B* 1998, **102**, 3216.
- A. G. Kontos, A. I. Kontos, D. S. Tsoukleris, V. Likodimos, J. Kunze, P. Schmuki and P. Falaras, *Nanotechnology* 2009, **20**, 045603.
- Z. Topalian, B. I. Stefanov, C. G. Granqvist and L. Österlund, *J. Catalysis* 2013, **307**, 256.
- A. Vittadini, A. Selloni, F. P. Rotzinger and M. Grätzel, *Phys. Rev. Lett.* 1998, **81**, 2954.
- G. S. Herman, Z. Dohnálek, N. Ruzycki and U. Diebold, *J. Phys. Chem. B* 2003, **107**, 2788.
- K. Furosawa, K. Takashi, S. H. Cho, H. Kumagai, K. Midorikawa and M. Obara, *J. Appl. Phys.* 2000, **87**, 1604.
- M. Kamei and T. Mitsuhashi, *Surf. Sci.* 2000, **463**, 609.
- F. Pan, K. Wu, H. Li, G. Xu and W. Chen, *Chem. Eur. J.* 2014, **46**, 15095.
- K. Chen, Z. Jiang, J. Qin, Y. Jiang, R. Li, H. Tang and X. Yang, *Ceram. Int.* 2014, **40**, 16823.
- N. Sutradhar, A. K. Biswas, S. K. Pahari, B. Ganguly and A. B. Panda, *Chem. Commun.* 2014, **50**, 11529.
- E. Grabowska, M. Diak, M. Marchelek and A. Zaleska, *Appl. Catal. B* 2014, **156-157**, 213.
- H. G. Yang, C. H. Sun, S. Z. Qiao, J. Zou, G. Liu, S. C. Smith, H. M. Cheng and G. Q. Lu, *Nature* 2008, **453**, 638.
- U. Diebold, *Surf. Sci. Rep.* 2003, **48**, 53.
- M. V. Dozzi and E. Selli, *Catalysts* 2013, **3**, 455.
- X. Q. Gong and A. Selloni, *J. Phys. Chem. B* 2006, **109**, 19560.
- T. Tachikawa, S. Yamashita and T. Majima, *J. Am. Chem. Soc.* 2011, **133**, 7197.
- S. K. Wallace and K. P. McKenna, *J. Phys. Chem. C* 2015, **119**, 1913.
- D. G. Howitt and A. B. Harker, *J. Mater. Res.* 1987, **2**, 201.
- P. Singh and D. Kaur, *Physica B* 2010, **405**, 1258.
- K. Eufinger, D. Poelman, H. Poelman, R. De Gryse and G. B. Marin, *J. Phys. D* 2007, **40**, 5232.
- S. Sério, M. E. Melo Jorge, M. J. P. Maneira and Y. Yunes, *Mat. Chem. Phys.* 2011, **126**, 73.
- B. Stefanov and L. Österlund, *Coatings* 2014, **4**, 587.
- B. I. Stefanov, C. G. Granqvist and L. Österlund, *J. Phys. Conf. Ser.* 2014, **559**.
- D. Le Bellac, G. A. Niklasson and C. G. Granqvist, *J. Appl. Phys.* 1995, **77**, 6145.
- D. Depla and S. Mahieu, editors "Reactive sputter deposition", Springer, Berlin, Heidelberg, 2008.
- W. Kraus, G. Nolzeb, *J. Appl. Cryst.*, 1996, **29**, 301.
- W. A. Dollase, *J. Appl. Cryst.* 1986, **19**, 205.
- E. Zolotoyabko, *J. Appl. Cryst.* 2009, **42**, 513.
- B. I. Stefanov, N. V. Kaneva, G. Li Puma and C. D. Dushkin, *Colloid. Surf. A* 2011, **382**, 219.
- M. Horn, C. F. Schwerdtfeger and E. P. Meagher, *Z. Kristallogr.* 1972, **136**, 273.
- R. Swanepoel, *J. Phys. E Sci. Instrum.* 1983, **16**, 1214.
- H. K. Pulker, *Appl. Optic.* 1979, **18**, 1969.
- W. J. Anthony, R. A. Bideaux, K. W. Bladh, M. C. Nichols, *Handbook of Mineralogy*; Mineralogical Society of America: <http://www.handbookofmineralogy.org/>
- A. Anders, *Thin Solid Films* 2010, **518**, 4087.

Figure 1. Schematic drawings of (a) experimental setup for preparation of TiO₂ thin films by magnetron sputtering, (b) anatase TiO₂ films in as-deposited, amorphous state and after annealing in air at 500°C to obtain randomly oriented crystallites (at low P_{O_2}) or a high degree of <001> preferential orientation (high P_{O_2}), (c) cross-section transmission electron microscopy (TEM) image of a highly oriented film, and (d) associated micro-diffraction pattern showing <001> orientation along the growth direction.

Figure 2. MD distribution functions, $W(\alpha)$, as a function of the angle α , between the <001> direction and the growth direction of the film, for five different values of the MD parameter. The vertical dashed grey lines show the integration range, $-\pi/6 < \alpha < \pi/6$ ($-30^\circ < \alpha < 30^\circ$), used for calculation of η_{001} and the hatched area shows the more conservative range, $-\pi/18 < \alpha < \pi/18$ ($-10^\circ < \alpha < 10^\circ$), which we assume will lead to exposed {001} facets on the surface of the films and is used for calculation of A_{001} . See main text for details.

Figure 3. Photographic images of as-deposited anatase TiO₂ films prior to heat-treatment. Films deposited at low oxygen partial pressure P_{O_2} are substoichiometric and almost black. The films gradually turn transparent at high P_{O_2} and concomitantly attain stoichiometric composition. All post-heat treatment films turned transparent.

Figure 4. O₂ partial pressure, P_{O_2} , vs. amount of <001> preferential film orientation, η_{001} for sputter deposition from two differently aged Ti targets. Lines are drawn to guide the eye.

Figure 5. AFM images of anatase TiO₂ films sputter deposited at increasing values of the oxygen partial pressure P_{O_2} . The root mean square surface roughnesses are listed in Table 1. Images marked with asterisk were obtained from films sputtered with an eroded target (see text).

Figure 6. X-ray diffractograms for anatase TiO₂ films with controlled amount of preferential <001> orientation. Numbers to the right indicate the amount of <001> orientation (see text). Red bars mark positions for all intensive XRD reflections of anatase TiO₂, as obtained from literature data.²⁸

Figure 7. Transmission spectrum of a film with $\eta_{001} = 38\%$. Red and blue dotted lines show the envelope functions, obtained by fitting a spline to the respective minima and maxima of the interference fringes.

Figure 8. Concentration profile, C in the solution, as a function of time, for the photocatalytic degradation of MB on a TiO₂ film. First 40 min represent adsorption in darkness, followed by 80 min of UV illumination. Red curve represents an isothermal fit; blue line represents pseudo first-order kinetics. Lines are added to guide the eye only; the actual fits are done with recalculated data, as described in the text.

Figure 9. Semi-logarithmic plots of normalized MB concentration vs. reaction time for three samples with increasing values of η_{001} demonstrating first-order reaction kinetics.

Figure 10. MB photo-degradation rate, k_{MB} , as a function of the exposed {001} area, A_{001} (see text). Dashed curve shows the best fit according to eq. 11.

Table 1. Summary of structural, optical and photocatalytic properties of anatase TiO₂ films, showing oxygen partial pressure (P_{O_2}), sputtering power (P), March-Dollase parameter (MD), fraction of preferential <001> orientation (η_{001}), film thickness (d), mean crystallite size (d_{xrd}), packing density (ρ), refractive index (n), AFM roughness (r_{rms}), equilibrium methylene blue saturation concentration under dark conditions (C_{sat}^{MB} , expressed as part of the 1 ppm initial concentration in solution), and MB degradation rate (k_{MB}). Asterisks signify that the films were sputter deposited from aged targets (see Figure 4).

P_{O_2} , mTorr	P , W	MD	η_{001} , %	d , nm	d_{xrd} , nm	ρ , %	n	r_{rms} , nm	C_{sat}^{MB} , ppm	k_{MB} , $\times 10^{-3} \text{ min}^{-1}$
0.64	211	0.97	2	574	24	93	2.36	1.3	0.27	0.96
0.56*	192	0.89	7	518	26	91.4	2.32	1.4	0.25	1.02
0.95	223	0.81	12	579	26	91	2.31	1.1	0.3	1.00
0.8*	207	0.66	23	485	25	89.8	2.28	1.3	0.31	1.31
1.25	244	0.64	25	664	22	86.5	2.20	1.4	0.28	1.43
0.95*	219	0.60	28	557	22	86	2.19	1.2	0.29	1.72
1.10*	233	0.53	35	474	21	85.1	2.17	1.3	0.29	2.27
1.53	291	0.49	38	697	18	81	2.08	1.6	0.28	2.49

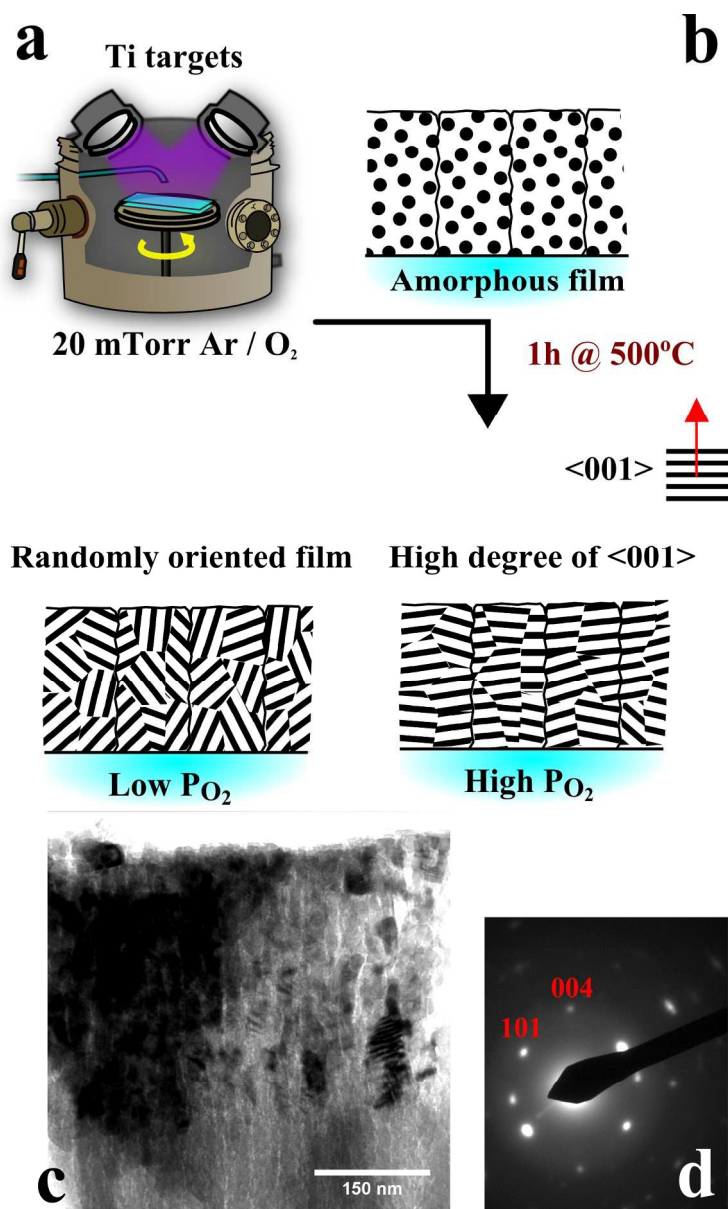


Figure 1. Schematic drawings of (a) experimental setup for preparation of TiO₂ thin films by magnetron sputtering, (b) anatase TiO₂ films in as-deposited, amorphous state and after annealing in air at 500°C to obtain randomly oriented crystallites (at low P_{O₂}) or a high degree of <001> preferential orientation (high P_{O₂}), (c) cross-section transmission electron microscopy (TEM) image of a highly oriented film, and (d) associated micro-diffraction pattern showing <001> orientation along the growth direction.
140x227mm (300 x 300 DPI)

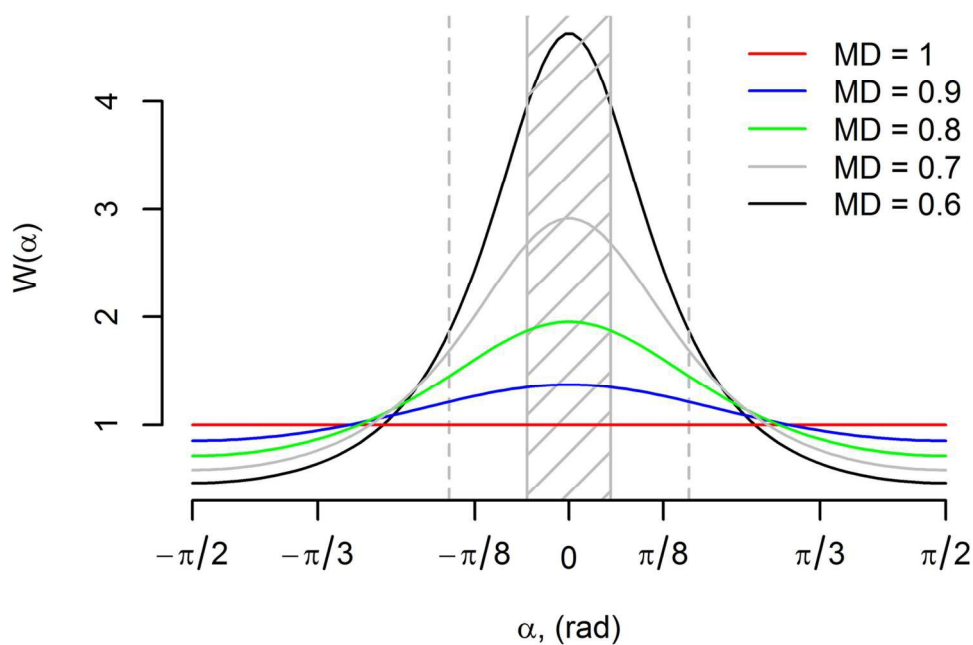


Figure 2. MD distribution functions, $W(\alpha)$, as a function of the angle α , between the $\langle 001 \rangle$ direction and the growth direction of the film, for five different values of the MD parameter. The vertical dashed grey lines show the integration range, $-\pi/6 < \alpha < \pi/6$ ($-30^\circ < \alpha < 30^\circ$), used for calculation of η_{001} and the hatched area shows the more conservative range, $-\pi/18 < \alpha < \pi/18$ ($-10^\circ < \alpha < 10^\circ$), which we assume will lead to exposed $\{001\}$ facets on the surface of the films and is used for calculation of A_{001} . See main text for details.

63x45mm (600 x 600 DPI)

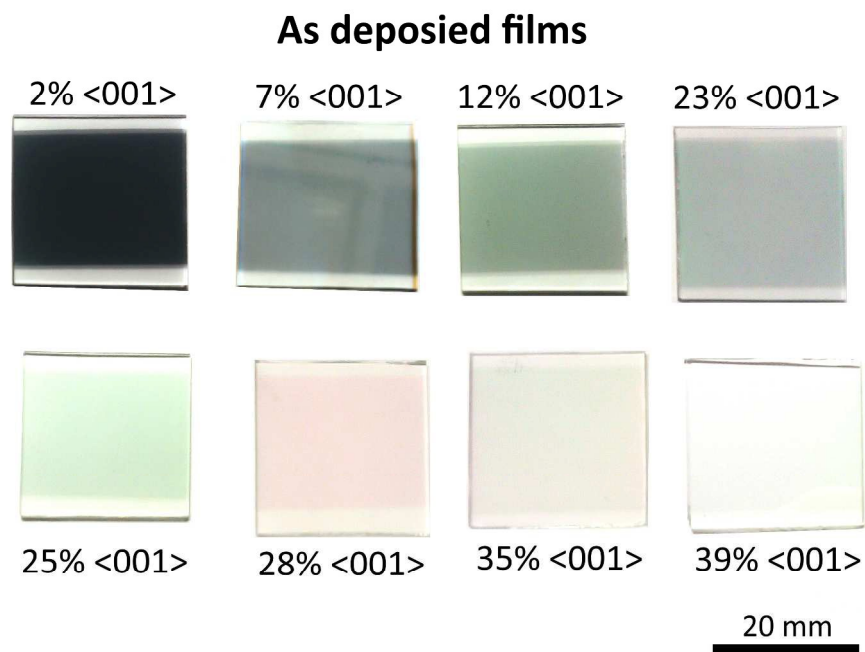


Figure 3. Photographic images of as-deposited anatase TiO₂ films prior to heat-treatment. Films deposited at low oxygen partial pressure P_{O_2} are substoichiometric and almost black. The films gradually turn transparent at high P_{O_2} and concomitantly attain stoichiometric composition. All post-heat treatment films turned transparent.
254x169mm (300 x 300 DPI)

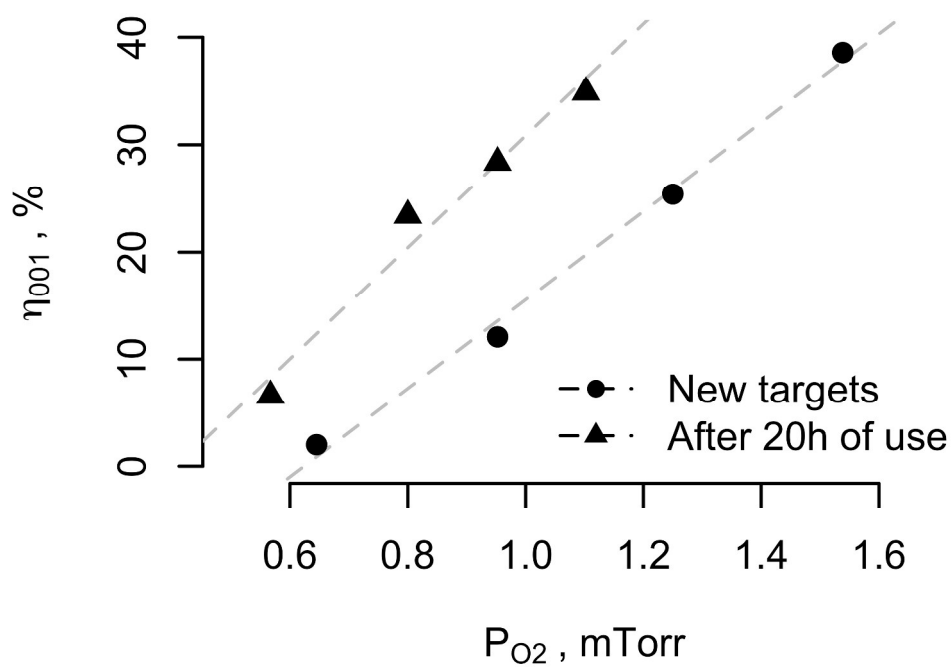


Figure 4. O_2 partial pressure, P_{O_2} , vs. amount of $\langle 001 \rangle$ preferential film orientation, η_{001} for sputter deposition from two differently aged Ti targets. Lines are drawn to guide the eye.
1110x833mm (72 x 72 DPI)

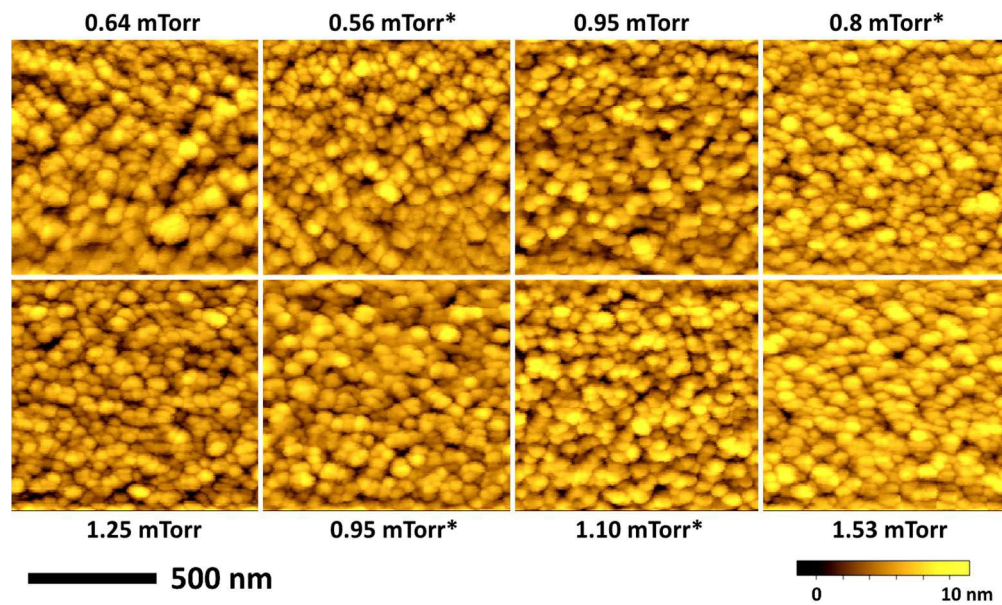


Figure 5. AFM images of anatase TiO_2 films sputter deposited at increasing values of the oxygen partial pressure P_{O_2} . The root mean square surface roughnesses are listed in Table 1. Images marked with asterisk were obtained from films sputtered with an eroded target (see text).
383x232mm (96 x 96 DPI)

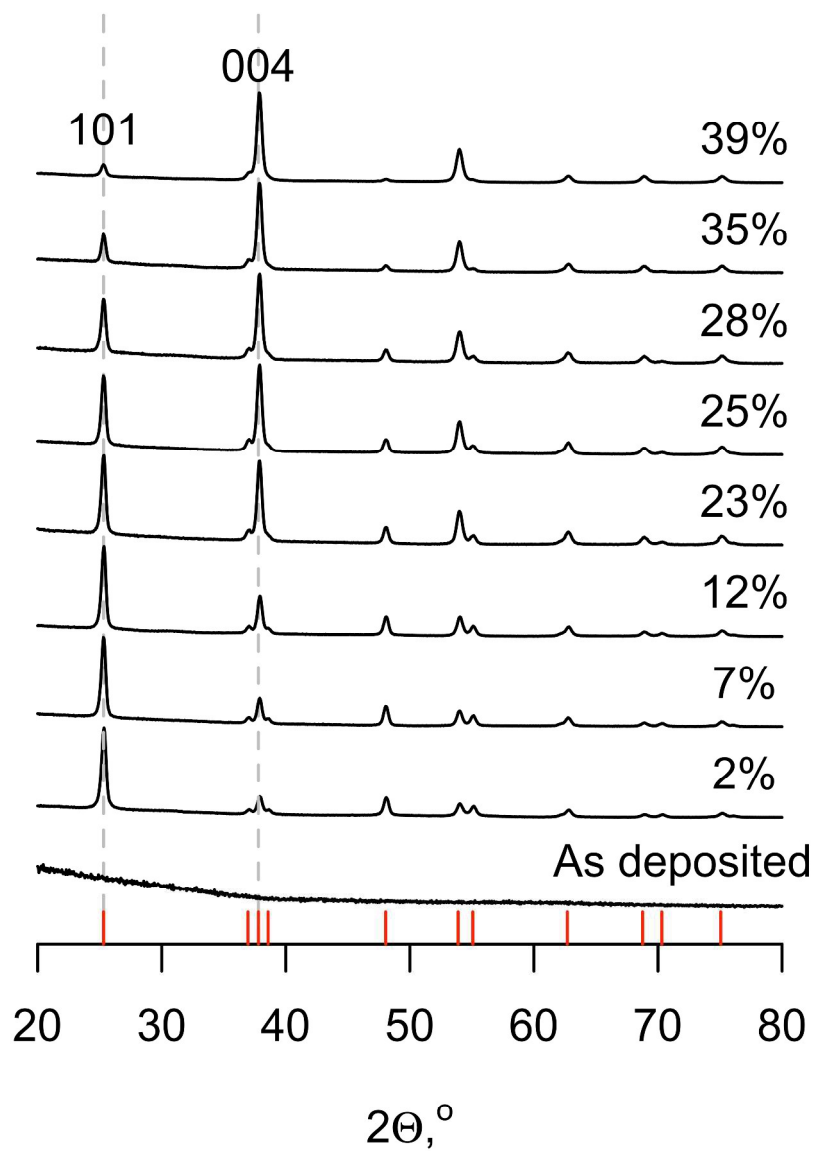


Figure 6. X-ray diffractograms for anatase TiO₂ films with controlled amount of preferential <001> orientation. Numbers to the right indicate the amount of <001> orientation (see text). Red bars mark positions for all intensive XRD reflections of anatase TiO₂, as obtained from literature data.²⁸
1097x1444mm (72 x 72 DPI)

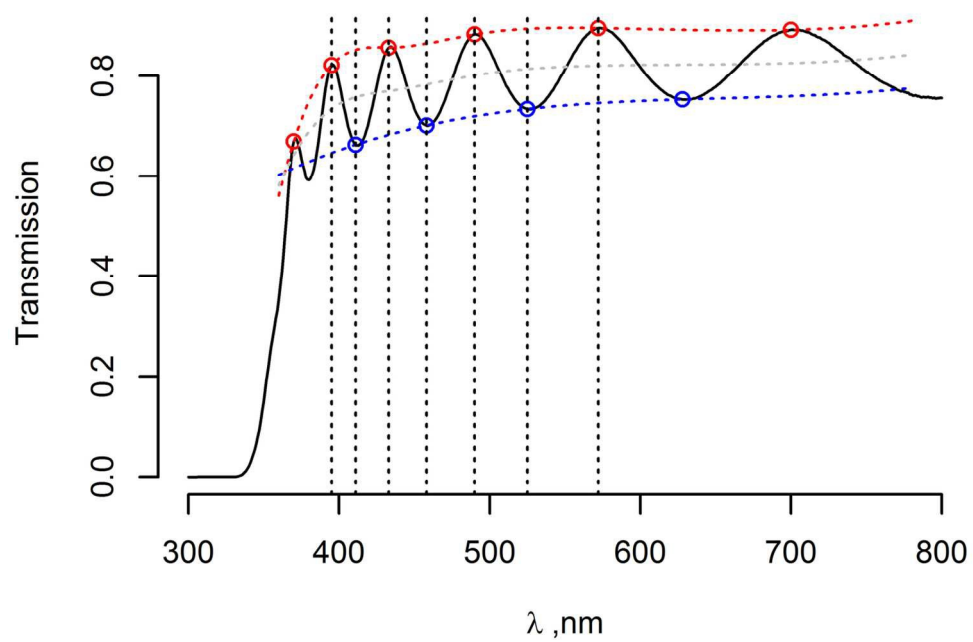


Figure 7. Transmission spectrum of a film with $\eta_{001} = 38\%$. Red and blue dotted lines show the envelope functions, obtained by fitting a spline to the respective minima and maxima of the interference fringes.
63x45mm (600 x 600 DPI)

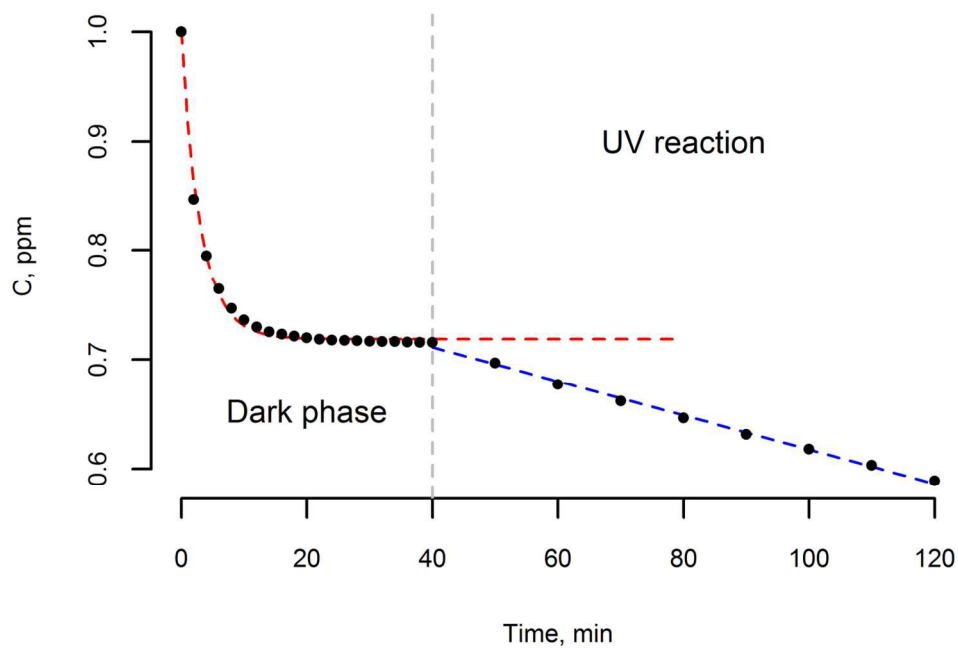


Figure 8. Concentration profile, C in the solution, as a function of time, for the photocatalytic degradation of MB on a TiO_2 film. First 40 min represent adsorption in darkness, followed by 80 min of UV illumination. Red curve represents an isothermal fit; blue line represents pseudo first-order kinetics. Lines are added to guide the eye only; the actual fits are done with recalculated data, as described in the text.
63x45mm (600 x 600 DPI)

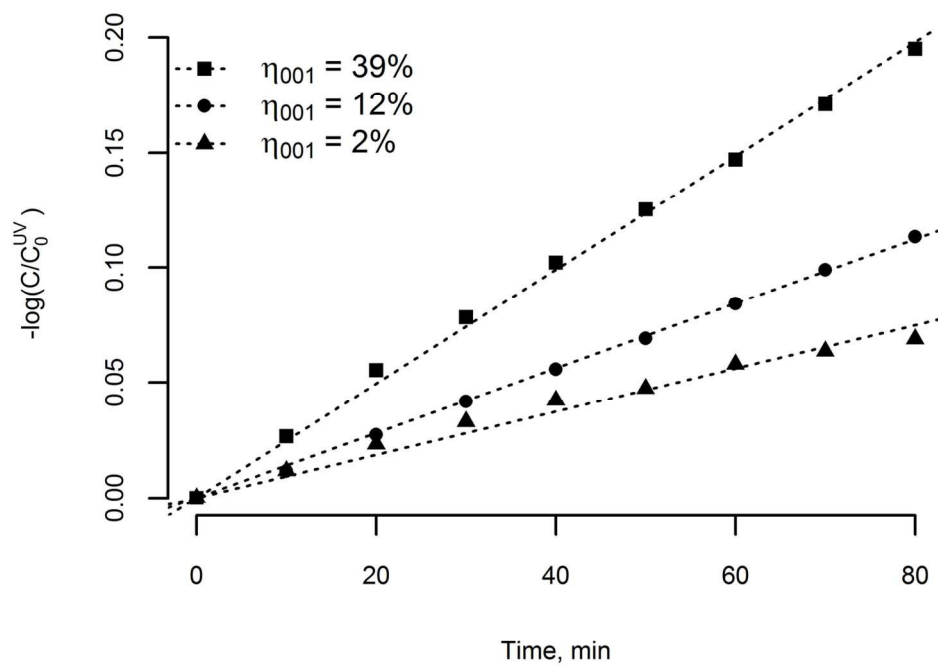


Figure 9. Semi-logarithmic plots of normalized MB concentration vs. reaction time for three samples with increasing values of η_{001} demonstrating first-order reaction kinetics.
63x45mm (600 x 600 DPI)

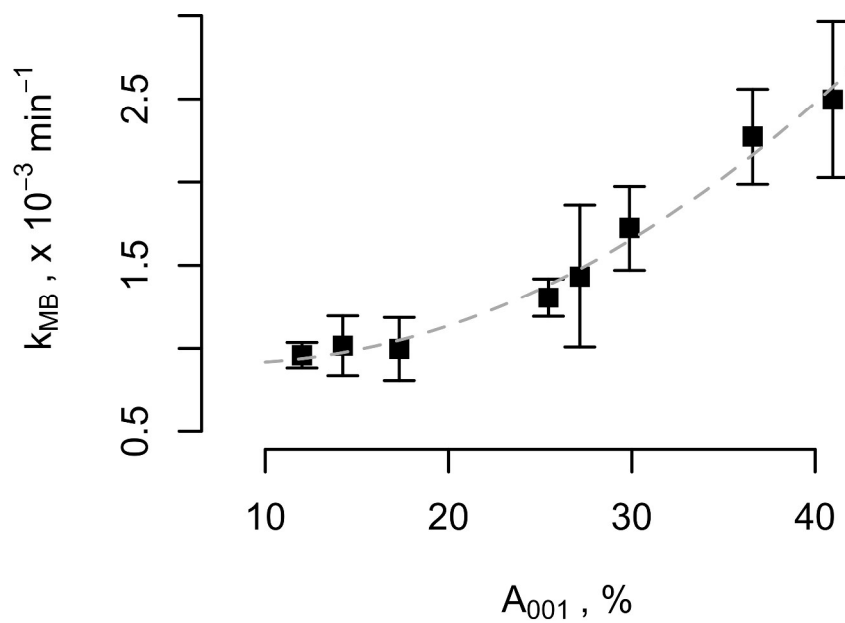
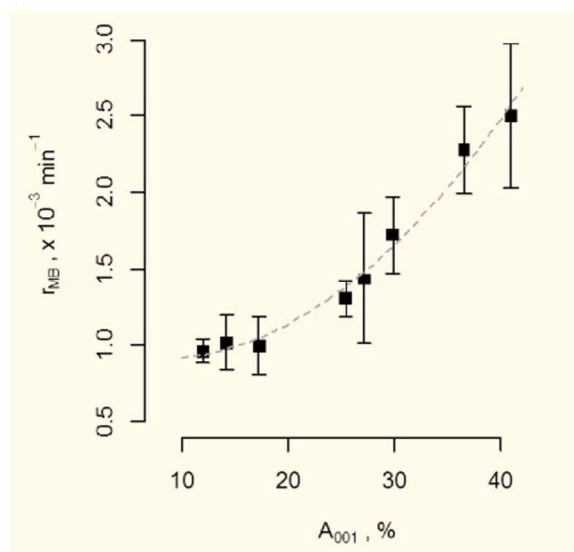
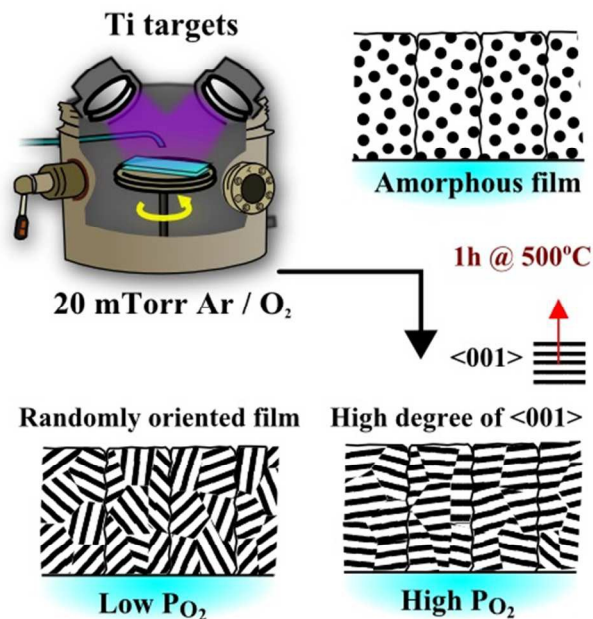


Figure 10. MB photo-degradation rate, k_{MB} , as a function of the exposed {001} area, A_{001} (see text). Dashed curve shows the best fit according to eq. 11.
1180x888mm (72 x 72 DPI)



We demonstrate a quantitative relation between exposed crystal surfaces and photocatalytic activity of nanocrystalline anatase TiO₂ films prepared by reactive DC magnetron sputtering. The films were deposited in Ar/O₂ atmosphere with the partial O₂ pressure as control parameter and characterized with AFM, TEM and XRD, from which the degree of preferential <001> orientation and exposed facets were determined. Photocatalytic degradation test with methylene blue dye shows that the photocatalytic reaction rate increases approximately with the square of the fraction of <001> oriented surfaces, with about eight times higher rate on the {001} surfaces, than on {101}, thus quantifying the effect of crystal facet abundance on the photocatalytic activity of anatase TiO₂.